Carbon nanotube supported platinum–palladium nanoparticles for formic acid oxidation

Olumide Winjobi[a], Zhiyong Zhang[a], Changhai Liang[b], Wenzhen Li[a,*]

[a] Department of Chemical Engineering, Michigan Technological University, 1400 Townsend Drive, Houghton, MI 49931, USA
[b] State Key Laboratory of Fine Chemicals, Dalian University of Technology, Dalian, China

ARTICLE INFO

ABSTRACT

Pt, Pd and Pt_xPd_y alloy nanoparticles (Pt_1Pd_1, Pt_1Pd_3, atomic ratio of Pt to Pd is 1:1, 1:3, respectively) supported on carbon nanotube (CNT) with high and uniform dispersion were prepared by a modified ethylene glycol method. Transmission electron microscopy images show that small Pt and Pt_xPd_y nanoparticles are homogeneously dispersed on the outer walls of CNT, while Pd nanoparticles have some aggregations and comparatively larger particle size. The average particle sizes of Pt/CNT, Pt_1Pd_1/CNT, Pt_1Pd_3/CNT and Pd/CNT obtained from the Pt/Pd (2 2 0) diffraction peaks in the X-ray diffraction patterns are 2.0, 2.4, 3.1 and 5.4 nm, respectively. With increasing Pd amount of the catalysts, the mass activity of formic acid oxidation reaction (FAOR) on the CNT supported catalysts increases in both cyclic voltammetry (CV) and chronoamperometry (CA) tests, although the particle size gets larger (thus, the relative surface area gets smaller). The CV study indicates a 'direct oxidation pathway' of FAOR occurred on the Pd surface, while on the Pt surface, the FAOR goes through 'CO_{ads} intermediate pathway'. Pd/CNT demonstrates 7 times better FAOR mass activity than Pt/CNT (2.3 mA/mgPd vs. 0.33 mA/mgPt) at an applied potential of 0.27 V (vs. RHE) in the CA test.

1. Introduction

Proton exchange membrane (PEM) based direct formic acid fuel cells (DFAFCs) have recently attracted enormous attention, due to their unique advantages, such as (1) DFAFCs have a high theoretical open circuit potential, e.g. emf of 1.450 V (compared to 1.229 V for H_2-proton exchange membrane fuel cells and 1.190 V for direct methanol fuel cells at room temperature; (2) formic acid is a non-toxic liquid fuel; (3) formic acid has a lower cross-over flux than methanol and ethanol; (4) although the neat energy density of formic acid (2086 Wh/L) is lower than that of methanol (4690 Wh/L), high concentrated formic acid can be used as fuel, e.g. 20 M (70 wt%), compared to low concentrated methanol, e.g. 1–2 M, therefore, formic acid carries more energy per volume than methanol; (5) formic acid itself is an electrolyte, thus, it can facilitate proton transport within anode compartment [1–11]. For the electro-oxidation of hydrogen, low carbon-chain aliphatic alcohol, such as methanol and ethanol, Pt is the primary catalyst to attain a high activity. For the formic oxidation reaction (FAOR), Pd has been found to perform better than Pt [2–7,10]. Waszczuk et al. reported that Pd-skin layer decorated Pt black shows two magnitudes higher FAOR activity than Pt black in chronoamperometry tests [3]. Pd

alloys with other elements, such as vanadium (V), modium (Mo) and gold (Au) show improved FAOR stability than pure Pd [6]. Pd particle size effect was also investigated, and a volcano curve was found, with an optimized Pd particle size of 5–7 nm [8]. Both geometric effect (ratio of crystallographic facets (1 1 1) to (1 0 0)) [8] and electronic effect [9] were provided to explain this structure-sensitive reaction.

Although unsupported noble/noble alloy catalysts, such as Pt, Pd and PtRu black, were investigated to study the reaction mechanisms of electrocatalysis, supported electrocatalyst is a practical means to achieve high utilization of expensive noble metals and to maintain good life-time. Carbon nanotubes (CNTs) – a new allotrope of carbon – have attracted enormous attention owing to their unique electronic and mechanical properties [12–14]. CNTs, aligned carbon porous arrays, carbon nanofibers, and carbon nanohorns work as electrocatalyst supports, and show promising electrocatalytic activity and better fuel cell performance [15–34].

In the past years, a simple ethylene glycol (EG) reduction method has been developed to prepare carbon black and CNTs supported Pt-based electrocatalysts, such as Pt [20–26,35–37] and PtFe [27] for oxygen reduction reaction, PtRu for methanol oxidation reaction [28], PtSn for ethanol oxidation reaction [29,30], and Pt and PtPd for formic acid oxidation [31–34]. This method does not involve any surfactants (e.g. polyvinylpyrrolidone, PVP) as stabilizers, and it is very simple and easy to scale up. The EG can be easily washed away by DI water. These electrocatalysts have small particle size (large

electrochemical surface area), narrow particle size distribution (2–5 nm), and uniform dispersion on carbon supports. Compared with traditional carbon black support, CNTs supported electrocatalysts show higher electrocatalytic activity [20–34], i.e. PtRu/double walled carbon nanotube catalyst demonstrated more than 3 times better MOR than PtRu/C [28]. They also exhibit improved durability and stability [35,36]. Our previous work shows almost 80% of Pt surface area was lost for Vulcan XC-72 after 168 h oxidation treatment, while only 37% was observed for multi-walled CNT [35]. In this paper, we investigated a modified EG method to prepare CNT supported Pt, Pd and Pt_xPd_y alloy catalysts, X-ray diffraction (XRD) and transmission electron microscopy (TEM) were used to characterize the catalyst particle size and size distribution. The formic acid oxidation activities on these CNT supported catalysts were evaluated by cyclic voltammetry and chronoamperometry tests.

2. Experimental

2.1. Catalyst preparation

Carbon nanotubes were kindly provided by Cheaptube Inc. and produced by a chemical vapor deposition (CVD) approach. Most CNTs have a diameter of 20–30 nm and length of 1–5 μm. The CNTs used in this paper were oxidized by an acid mixture of 2.0 M H_2SO_4–4.0 M HNO_3 under refluxing condition at 100 °C for 6 h, in order to produce functional groups on the outer wall surface of CNT [22]. Four CNT supported Pt_xPd_y catalysts with different PtPd ratios were prepared: Pt/CNT, Pt_1Pd_1/CNT (atomic ratio of Pt to Pd is 1:1), Pt_1Pd_3/CNT (atomic ratio of Pt to Pd is 1:3) and Pd/CNT. All the catalysts have a metal (Pt + Pd) loading of 30 wt%. The preparation was based on a self-developed EG method [22], which can be briefly described as follows: the surface oxidized CNT (226 mg) was suspended in an ethylene glycol solution and treated in an ultrasonic bath to form an uniform ink. Then an EG solution of hexachloroplatinic acid (H_2PtCl_6) or palladium nitrate ($Pd(NO_3)_2$), or their mixture was added drop wise, under vigorously stirred conditions for 2 h. A solution of 1.0 M NaOH (in EG) was added to adjust the pH of the synthesis solution to above 13, and then the mixture was heated at 135 °C for 3 h to reduce the Pt completely. The whole synthesis system has a water content of 10 vol.%. After cooling down to room temperature, the pH of the synthesis system was adjusted to 2–3 by 0.1 M HCl. The whole preparation process was conducted under flowing argon. After filtration, washing, and drying at 70 °C for overnight, the CNT supported catalyst was finally obtained. The filtrated solvent was transparent with light yellow color, which indicates most of Pt and Pd precursors were reduced during the synthesis process.

2.2. Catalyst characterization

Samples for TEM analysis were prepared by depositing one drop of diluted catalyst dispersion in ethanol on an amorphous carbon copper grid. Images were obtained by a JEOL 2010 (operating voltage of 200 kV). Energy dispersive X-ray spectroscopy (EDX) was conducted with the TEM instrument. Samples for XRD analysis were prepared by packing a thin film of CNT catalyst sample on an amorphous glassy holder. XRD patterns were collected by a Scintag XDS-2000 θ/θ diffractometer with Cu Kα radiation (λ = 1.5418 Å), the tube current is 40 mA and tube voltage is 40 kV.

2.3. Electrocatalysis activity tests

A conventional three-electrode cell setup (Pine Instrument) with a glassy carbon working electrode (GCE), a reversible hydrogen reference electrode (Hydroflex®, Gaskatel GmbH) and a Pt foil counter electrode, connected with a potentiostat (Princeton
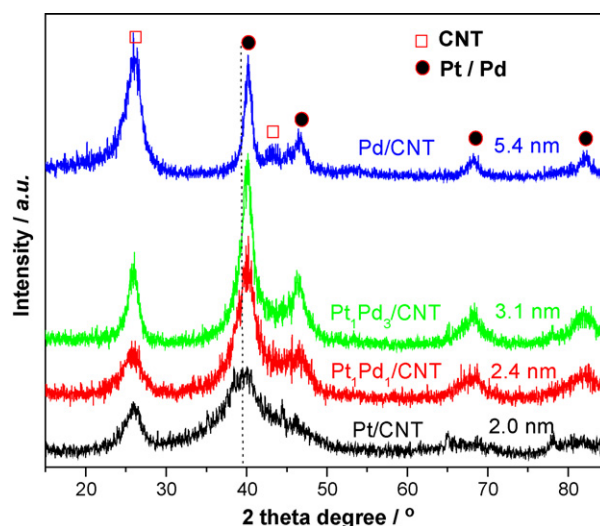

Fig. 1. Powder XRD patterns of Pt/CNT, Pt_1Pd_1/CNT, Pt_1Pd_3/CNT and Pd/CNT catalysts.

Applied Research, VMC-2) was used for the electrochemical tests on the Pt_xPd_y/CNT catalysts. 2 mg Pt_xPd_y/CNT was dissolved in 2 mL ethanol and ultrasonic treated for 5 min. A 20 μL suspension was dropped on the surface of glassy carbon (area: 0.1962 cm^2, diameter: 5 mm), subsequently covered by a 10 μL of 0.05 wt% Nafion. The Pt or Pd metal loading on GCE is around 30.6 μg/cm^2. The cyclic voltammetry was scanned 20 cycles from 0 to 1.2 V at the scan rate of 50 mV/s under a high purity nitrogen (99.999%) saturated atmosphere. The choronamperometry test was then conducted at 0.27 V vs. RHE for 2.78 h (10,000 s). After the choronamperometry test, a CV with 20 cycles was performed and the last cycle was reported. As a control sample, a commercial Pt/C catalyst (E-TEK, 20 wt%) was prepared and tested by CV, the Pt loading on GCE keeps at 30.6 μg/cm^2. The working electrolyte is 0.5 M H_2SO_4 + 0.5 M HCOOH for both CV and CA tests. All the tests were conducted at room temperature and ambient pressure, and all potentials were reported vs. RHE. Each catalyst sample was made to catalyst ink, deposited on GC, and then conducted electrochemical tests for 3 times. The median data was reported, the deviation of three tests is less than 5%.

3. Results and discussion

The powder XRD patterns of Pt/CNT, Pt_1Pd_1/CNT, Pt_1Pd_3/CNT and Pd/CNT catalysts with a metal loading of 30 wt% are shown in Fig. 1. The strong diffraction peaks at 26.5° and 42.4° are attributed to the hexagonal graphite structure (0 0 2) and (1 0 0), which suggests CNT has a high graphite structure and good electrical conductivity. The Pt/Pd diffraction peaks show that all catalysts have a face centered cubic (fcc) crystal structure. The diffraction peaks at 2θ = 39.7°, 46.2°, 67.4° and 81.2° can be assigned to Pt (1 1 1), (2 0 0), (2 2 0) and (3 1 1) diffraction peaks, respectively. The isolated Pt/Pd (2 2 0) peaks were chosen to calculate the average metal crystalline particle sizes using the Debye–Scherrer formula [22]. They are 2.0, 2.4, 3.1 and 5.4 nm for the Pt/CNT, Pt_1Pd_1/CNT, Pt_1Pd_3/CNT and Pd/CNT, respectively. By using the EG synthesis method, the average particle size increases with increasing Pd ratio of the catalysts. Furthermore, with more Pd amount of the catalyst, the diffraction peaks shift to right. A dash line is shown in Fig. 1, which marks the 2θ position of Pt (1 1 1) peak. The lattice parameters of Pt/CNT, Pt_1Pd_1/CNT, Pt_1Pd_3/CNT and Pd/CNT samples based on Pt/Pd (2 2 0) diffraction peaks are 3.924, 3.909, 3.900 and 3.891 Å, respectively. Note that the lattice parameter of Pt (fcc) is 3.923 Å,
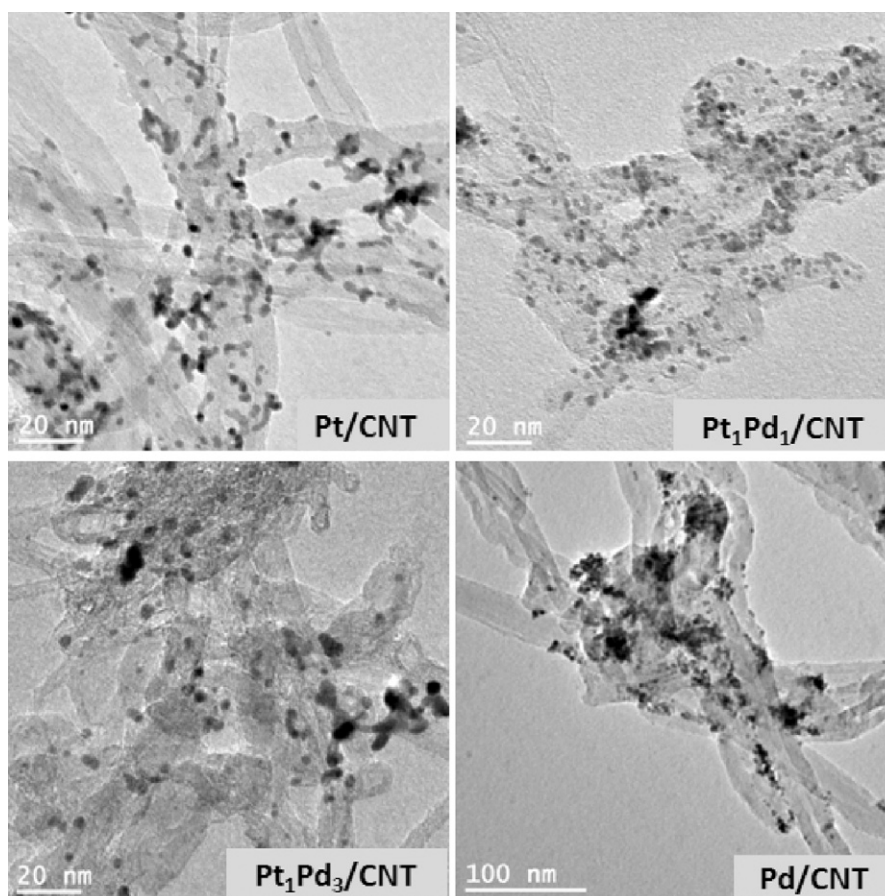
Fig. 2. TEM images of Pt/CNT, Pt_1Pd_1/CNT, Pt_1Pd_3/CNT and Pd/CNT catalysts.

and that of Pd (fcc) is 3.890 Å from JCPDS. The Pt_xPd_y nanoparticles have very close crystalline structure as their bulk metal counterparts. The Pt_1Pd_3/CNT has a lattice parameter of 3.900 Å, which is close to the lattice parameter of 3.902 Å for the Pd_3Pt/carbon black (XC-72C, atomic ratio of Pt to Pd is 1:3) that we previously reported in Ref. [38]. This suggests that the CNT has little influence on the metal alloy degree using the EG synthesis method.

Typical TEM images of Pt/CNT, Pt_1Pd_1/CNT, Pt_1Pd_3/CNT and Pd/CNT are shown in Fig. 2. For Pd/CNT, Pd nanoparticles are randomly dispersed on the CNT surface, and some of them tend to agglomerate and connect together. The particle size of Pd is in a range of 4–10 nm, centered at 6.2 nm. In contrast, Pt/CNT has very small Pt particles uniformly dispersed on the CNT surface, the average particle size is around 2.8 nm. Our TEM images are in a good agreement with the XRD results. It has been reported that commercial Pd/C catalyst (20 wt%, E-TEK) also has a larger particle size than Pt/C (20 wt%, E-TEK): 3.1 nm *vs.* 2.3 nm based on TEM images [39]. Xia group systematically studied synthesis of Pt and Pd nanostructures. They found Pd tends to form twinned or multiple twinned seeds, while Pt prefers to form single crystal seeds, due to their different chemical natures. As a result, twinned or multi-twinned Pd nanostructures can be produced [40]. This perhaps can help us to explain why Pd/CNT has some agglomerations, while highly dispersed Pt nanoparticles are prevalent. TEM–EDX shows that the atomic ratio of Pt to Pd is around 1:1 and 1:2.5 for Pt_1Pd_1/CNT and Pt_1Pd_3/CNT, respectively. They are close to the setting ratio of Pt to Pd in their precursors.

Electrochemical oxidation of formic acid on Pt_xPd_y/CNT catalysts was evaluated by the CV and CA tests. Before discussing the CV results, it is beneficial to briefly review formic acid oxidation reaction on Pt and Pd catalysts. There are two generally accepted

pathways for electro-oxidation of formic acid, differentiated by the intermediates involved. One is called 'direct oxidation pathway': formic acid oxidizes directly to CO_2 without passing through the chemisorbed intermediate. The other is called 'CO_{ads} intermediate pathway': formic acid oxidizes through a chemisorbed CO intermediate [3,8,9,41,42]. The two pathways are illustrated by the following two equations [3]:

$$HCOOH \rightarrow X \rightarrow CO_2 + 2e^- + 2H^+ \qquad (1)$$

$$HCOOH \rightarrow CO_{ads} + H_2O \qquad (2)$$
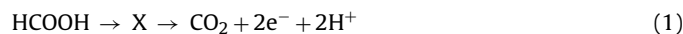
The *in situ* FTIR studies indicate that the reaction pathways of the FAOR on Pt (1 1 1) and Pd decorate Pt (1 1 1) single crystals are very different. While Pd has in the entire potential region (0–0.9 V *vs.* RHE) a propensity to break only the O–H bonds of the HCOOH molecule, Pt seems to have a propensity to break both the C–O and/or C–H bond (at low potentials) as well as the O–H bond (at high potentials). Consequently, HCOOH oxidation on Pd surface proceeds exclusively through the dehydrogenation reaction step, while at low potentials on Pt surface the dehydration reaction pathway is predominant [41]. Single crystal study also shows the onset potential of FAOR of Pt (1 1 1) (around 0.2 V *vs.* RHE, in 0.23 M HCOOH + 1 M $HClO_4$) is more negative than that of Pt (1 1 0) (ca. 0.6 V *vs.* RHE), but the FAOR activity on Pt (1 1 1) is much lower than that on Pt (1 1 0) [42].

Fig. 3 shows steady-state cyclic voltammograms of FAOR for the four Pt_xPd_y/CNT catalysts in 0.5 M HCOOH + 0.5 M H_2SO_4, with a sweep rate of 50 mV/s. Three distinct oxidation peaks: peak 1 in range of 0.27–0.44 V; peak 2 in range of 0.53–0.64 V, and peak 3 in range of 0.89–0.92 V are observed for the Pt_xPd_y/CNT catalysts, i.e. Pd/CNT has one big oxidation peak (peak 1, at 0.44 V) with a
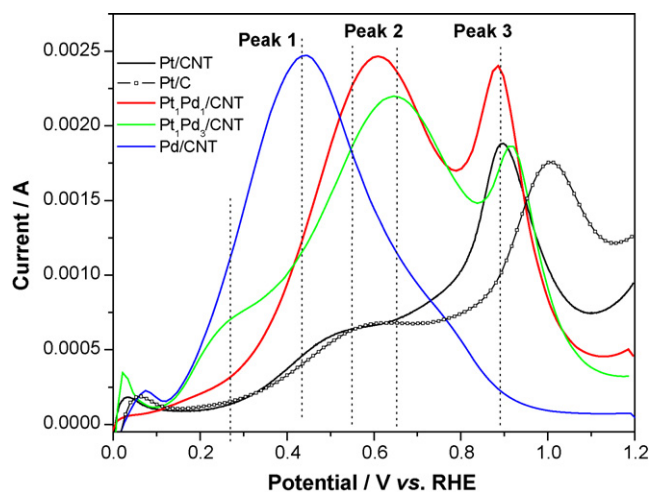
Fig. 3. Cyclic voltammograms of formic acid oxidation on Pt/CNT, Pt_1Pd_1/CNT, Pt_1Pd_3/CNT Pd/CNT and Pt/C (E-TEK) in 0.5 M H_2SO_4 + 0.5 M HCOOH, at a sweep rate of 50 mV/s, room temperature. Only the positive-going potential scans are reported.
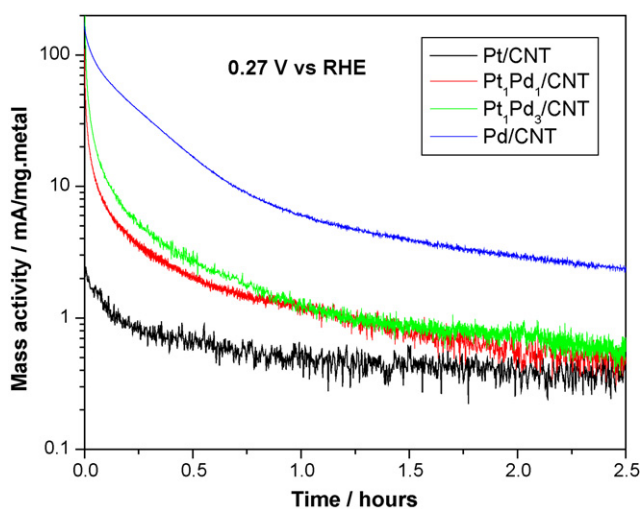

Fig. 4. Chronoamperometric activity of formic acid oxidation on Pt/CNT, Pt_1Pd_1/CNT, Pt_1Pd_3/CNT and Pd/CNT in 0.5 M H_2SO_4 + 0.5 M HCOOH, at 0.27 V *vs.* RHE, room temperature.

small shoulder peak (at 0.77 V). The Pt_1Pd_3/CNT has a small peak 1 at 0.26 V, and peak 2 (at 0.64 V) and peak 3 (0.92 V) with comparatively similar height (current density), while Pt/CNT has only peak 2 and peak 3—no peak 1 can be observed for Pt/CNT. Based on discussion above, the peak 1 can be assigned to direct oxidation of formic acid on Pd surface, while the peak 2 and peak 3 can be assigned to the oxidation of CO_{ads} intermediates exclusively on Pt surface. With increasing Pd-Pt ratio of the Pt_xPd_y/CNT catalysts, more Pd is on the catalyst surface, therefore, the peak 1 increases. With increasing Pt amount, peak 1 diminishes and the ratio of peak 3 to peak 2 increases. This may because the intrinsic activity of FAOR on Pt changes, when Pt is interacted (alloyed) with Pd. It could also be attributed to the changes in ratio of low index planes, i.e. Pt (1 1 1) to Pt (1 1 0) or Pt (1 1 1) to (1 0 0) with particle size decreasing. More characterization research should be conducted to elucidate the mechanisms. The onset potential for peaks 2 and 3 shifts negatively for self-prepared Pt/CNT compared to Pt/C (E-TEK), which suggests Pt/CNT has a slightly higher FAOR activity than Pt/C.

Chronoamperometry tests on Pt_xPd_y/CNT catalysts were shown in Fig. 4. At a constant voltage of 0.27 V (*vs.* RHE), the FAOR cur-

rents drop quickly and approach to a constant value. After 2 h, the pseudo 'stabilized' mass activity of Pt/CNT, Pt_1Pd_1/CNT, Pt_1Pd_3/CNT and Pd/CNT is 0.33, 0.67, 0.72, 2.3 mA/mg·metal, respectively. In the CV tests, the mass activity of Pt/CNT, Pt_1Pd_1/CNT, Pt_1Pd_3/CNT and Pd/CNT is 30, 50, 125, 200 mA/mg·metal at 0.27 V, respectively. The CV tests show same trend as the CA tests: with more Pd in the catalysts, the pseudo 'stabilized' FAOR mass activity on the Pt_xPd_y/CNT is improved. Pd/CNT exhibits 7 times higher mass activity than Pt/CNT. CV gives much higher mass activity (about two magnitudes) than the CA tests at 0.27 V, this is because CV is a steady-state test and the CO_{ads} poisons can be oxidized at a higher applied potential (e.g. >0.7 V *vs.* RHE), while the CO_{ads} poisons will gradually accumulate on the catalyst surface and deteriorate the catalyst activity in CA tests.

Elegant work on Pt black surface doped with Pd-skin layer can greatly improve the FAOR activity of Pt by two magnitudes [3]. However, in our study, we do not observe such great promotion effect, this may be due to their different surface catalytic structures, owing to different synthesis approaches. We adopted a wet-chemistry-based EG synthesis to achieve PtPd alloy structure (evidenced by XRD), and Ref. [3] used an electrochemical deposition approach to obtain a Pd-skin layer structure with modified electronic properties. Selvaraj et al. reported PtPd/SWNT (atomic ratio of Pt to Pd: 1:1) shows around 2 times higher FAOR mass activity than Pt/SWNT [34]. Our current study is consistent with their work. Furthermore, we demonstrated that with increasing Pd amount in the catalyst, the FAOR activity increases: Pd/CNT has 7 times higher FAOR mass activity than Pt/CNT. Our results are also consistent with Ref. [7], where the electrochemical deposited unsupported Pd catalyst shows higher FAOR activity than the PtPd (atomic ratio 1:1) and Pt catalysts. Zhou et al. prepared Pd/XC-72R catalysts with various particle sizes from 2.7 to 8.7 nm by altering the ratio of trisodium citrate (stabilizer) and $PdCl_2$ (Pd precursor). The Pd nanoparticles in the range of 5–7 nm have the highest specific activity to FAOR, owing to a good compromise between surface area and ratio of the (1 1 1) to (1 0 0) [8]. However, the mass activity of FAOR on Pd/XC-72R decreases with the Pd particle size increased from 2.72 to 8.67 nm. Our Pd/CNT catalyst has a comparatively large particle size of 5.4 nm (by XRD, 6.2 nm determined by TEM). Future research will be focused on developing new solution-phase synthesis method [43–45] for the preparation of Pd catalysts with smaller particle size (e.g. <4 nm) and special structures (e.g. Pt-core Pd-shell), which are expected to have enhanced FAOR activity. They are currently ongoing work in our lab.

4. Conclusions

Small Pt, Pd and Pt_xPd_y alloy nanoparticles with uniform dispersion supported on CNT were prepared through a modified ethylene glycol method. XRD patterns show that the average particle size of Pt/CNT, Pt_1Pd_1/CNT, Pt_1Pd_3/CNT and Pd/CNT is 2.0, 2.4, 3.1 and 5.4 nm, respectively, based on the Pt/Pd (2 2 0) diffraction peak using Sherrer formula. TEM images show that Pd nanoparticles are larger than Pt nanoparticles on CNT, and Pd nanoparticles tend to aggregate compared to small Pt nanoparticles. Formic acid oxidation reaction activities on these CNT supported electrocatalysts were measured by cyclic voltammetry and chronoamperometry tests. The results show that the mass activity of FAOR on these CNT supported catalysts increases with more Pd amount of the catalyst, although the particle size gets larger. The CV study indicates a 'direct oxidation pathway' of FAOR occurred on the Pd surface, while on the Pt surface, the FAOR goes through 'CO_{ads} intermediate pathway'. In the CA tests at an applied potential of 0.27 V, the mass activity of Pt/CNT, Pt_1Pd_1/CNT, Pt_1Pd_3/CNT and Pd/CNT is 0.33, 0.67, 0.72, 2.3 mA/mg·metal, respectively.

Acknowledgements

References

[1] M. Weber, T. Wang, S. Wasmus, R.F. Savinell, J. Electrochem. Soc. 143 (1996) 158.
[2] C. Rice, S. Ha, P. Masel, P. Waszczuk, A. Wiechowski, J. Power Sources 111 (2002) 83.
[3] P. Waszczuk, T.M. Barnard, C. Rice, R.I. Masel, A. Wiechowski, Electrochem. Commun. 4 (2002) 599.
[4] C. Rice, S. Ha, R.I. Masel, A. Wieckowski, J. Power Sources 115 (2003) 229.
[5] Y. Zhu, Z. Khan, R.I. Masel, J. Power Sources 139 (2005) 15.
[6] R. Larsen, J. Zakzeski, R.I. Masel, Electrochem. Solid State Lett. 8 (2005) 291.
[7] R.S. Jayashree, J.S. Spendelow, J. Yeom, C. Rastogi, N.A. Shannon, P.J.A. Kenis, Electrochim. Acta 50 (2005) 4674.
[8] W.J. Zhou, J.Y. Lee, J. Phys. Chem. C 112 (2008) 3789–3793.
[9] W.P. Zhou, A. Lewera, R. Larsen, R.I. Masel, P.S. Bagus, A. Wieckowski, J. Phys. Chem. B 110 (2006) 13393.
[10] Z.L. Liu, L. Hong, M.P. Tham, T.H. Lim, H.X. Jiang, J. Power Sources 161 (2006) 831.
[11] V. Mazumder, S.H. Sun, J. Am. Chem. Soc. 131 (2009) 4588.
[12] S. Iijima, Nature 354 (1991) 56.
[13] T.W. Ebbesen, P.M. Ajayan, Nature 358 (1992) 220.
[14] W.Z. Li, S.S. Xie, L.X. Qian, B.H. Chang, B.S. Zou, W.Y. Zhou, Science 274 (1996) 1701.
[15] G.L. Che, B.B. Lakshmi, E.R. Fisher, C.R. Martin, Nature 298 (1999) 760.
[16] S.H. Joo, S.J. Choi, I. Oh, J. Kwak, Z. Liu, O. Terasaki, R. Ryoo, Nature 412 (2002) 169.
[17] C.A. Bessel, K. Laubernds, N.M. Rodriguez, R.T.K. Baker, J. Phys. Chem. B 105 (2001) 1115.
[18] E.S. Steigerwalt, G.A. Deluga, D.E. Cliffel, C.M. Lukehart, J. Phys. Chem. B 105 (2001) 8097.
[19] T. Yoshitake, Y. Shimakawa, S. Kuroshima, H. Kimura, T. Ichihashi, Y. Kubo, D. Kasuya, K. Takahashi, F. Kokai, M. Yudasaka, S. Iijima, Phys. B: Condens. Matter 323 (2002) 124.
[20] W. Li, C. Liang, J. Qiu, W. Zhou, H. Han, Z. Wei, G. Sun, Q. Xin, Carbon 40 (2002) 791.
[21] Z. Lin, X.H. Lin, J.Y. Lee, W. Zhang, M. Han, L.M. Gan, Langmuir 10 (2002)4054.
[22] W. Li, C. Liang, W. Zhou, J. Qiu, Z. Zhou, G. Sun, Q. Xin, J. Phys. Chem. B 107 (2003) 6292.
[23] W. Li, C. Liang, W. Zhou, J. Qiu, H. Li, G. Sun, Q. Xin, Carbon 42 (2004) 436.
[24] W. Li, X. Wang, Z. Chen, M. Waje, Y. Yan, Langmuir 21 (2005) 9386.
[25] M.M. Waje, X. Wang, W. Li, Y. Yan, Nanotechnology 16 (2005) S395.
[26] L.S. Knupp, W. Li, O. Paschos, M. Murray, J. Snyder, P. Haldar, Carbon 46 (2008) 1276.
[27] W. Li, C. Liang, J. Qiu, H. Li, W. Zhou, G. Sun, Q. Xin, React. Kinet. Catal. Lett. 82 (2002) 235.
[28] W. Li, X. Wang, Z. Chen, M. Waje, Y. Yan, J. Phys. Chem. B 110 (2006) 15353.
[29] X. Zhao, W. Li, G. Sun, W. Zhou, L. Jiang, Q. Xin, B. Yi, G. Sun, Carbon 42 (2004) 3263.
[30] W. Zhou, Z. Zhou, S. Song, W. Li, G. Sun, P. Tsiakaras, Q. Xin, Appl. Catal. B: Environ. 46 (2003) 273.
[31] G.Y. Gao, D.J. Guo, H.L. Li, J. Power Sources 162 (2006) 1094.
[32] V. Selvaraj, M. Alagar, K.S. Kumar, Appl. Catal. B: Environ. 75 (2007) 129.
[33] S.D. Yang, X.G. Zhang, H.Y. Mi, X.G. Ye, J. Power Sources 175 (2008) 26.
[34] V. Selvaraj, A. Nirmala Grace, M.J.M. Alagar, J. Colloid Interface Sci. 333 (2009) 254.
[35] X. Wang, W. Li, Z. Chen, M. Waje, Y. Yan, J. Power Sources 158 (2006) 154.
[36] M. Waje, W. Li, Z. Chen, Y. Yan, ECS Trans. 31 (2006) 677.
[37] Z. Zhou, S. Wang, W. Zhou, G. Wang, L. Jiang, W. Li, S. Song, J. Liu, G. Sun, Q. Xin, Chem. Commun. 3 (2003) 394.
[38] H. Li, Q. Xin, W. Li, Z. Zhou, L. Jiang, S. Yang, G. Sun, Chem. Commun. 23 (2004) 2776.
[39] L. Jiang, A. Hsu, D. Chu, R. Chen, J. Electrochem. Soc. 156 (2009) B370.
[40] Y. Xiong, Y. Xia, Adv. Mater. 19 (2007) 3385.
[41] M. Arenz, V. Stamenkovic, T.J. Schmidt, P.N. Ross, N.M. Markovic, Phys. Chem. Chem. Phys. 5 (2003) 4242.
[42] N.M. Markovic, P.N. Ross, Surf. Sci. Rep. 45 (2002) 117.
[43] W. Li, P. Haldar, Electrochem. Commun. 11 (2009) 1195.
[44] W. Li, L. Xu, Z. Chen, Y. Yan, J. Power Sources 195 (2010) 2534.
[45] W. Li, P. Haldar, Electrochem. Solid State Lett. 13 (2010) B47.